

# Synthesis, Characterization and Antioxidant Study of Some Metal Ion Complexes with Azo 1-(2,4,6-trihydroxy-3-((3-hydroxyphenyl) diazenyl) phenyl) Ethan-1-one.

Areeg Malek Fadhel<sup>\*1</sup>  , Abbas Ali Salih Al Hamdani<sup>2</sup>  , Saad G. Mohamed<sup>3</sup>  

<sup>1</sup>Ministry of Education, Baghdad Education Directorate, Baghdad, Iraq.

<sup>2</sup>Department of Chemistry, Collage of Science for Women, University of Baghdad, Baghdad, Iraq.

<sup>3</sup>Mining and Metallurgical Engineering Department, Tabbin Institute for Metallurgical Studies, Cairo, Egypt.

\*Corresponding author.

Received 19/11/2023, Revised 14/01/2024, Accepted 16/01/2024, Published Online First 20/05/2024



© 2022 The Author(s). Published by College of Science for Women, University of Baghdad.

This is an open-access article distributed under the terms of the [Creative Commons Attribution 4.0 International License](https://creativecommons.org/licenses/by/4.0/), which permits unrestricted use, distribution, and reproduction in any medium, provided the original work is properly cited.

## Abstract

During a diazotization coupling reaction, an azo dye-ligand (H<sub>4</sub>L) was formed by combining 3-aminophenol and 2,4,6-trihydroxyacetophenone. This ligand was then allowed to react with several different metal ions (Mo (VI), Fe (III), Co (II), Cr (III), Ru (III) and Rh (III)), forming stable metal complexes with various geometries. The binding of the azo-dye group to the metal ions was detected through the M-N and M-O absorption bands in Fourier-transform-infrared, which indicated the involvement of nitrogen and oxygen. LC-MS spectra confirmed the molecular weights of the ligand and its complexes, and elemental analysis was also conducted. Electronic spectra were used to determine the geometries of the complexes. Furthermore, the thermal stability of some compounds and the existence of water molecules were detected using Differential Scanning Calorimetry (DSC) and Thermogravimetric analysis (TGA). The antioxidant effectiveness of these complexes was tested towards 2,2-Diphenyl-1-picrylhydrazyl (DPPH), a stable free radical that can be used to test the radical scavenging activity of reactive oxygen species. The order of inhibitory action of the ligand H<sub>4</sub>L and its minerals towards reactive oxygen species was determined to be (H<sub>4</sub>L > Ascorbic acid > Mo-Complex > Fe-Complex > Cr-Complex > Rh-Complex > Ru-Complex) at 30 minutes. The DPPH test involves reducing the odd electron of a nitrogen atom by receiving a hydrogen atom from antioxidants to form the corresponding hydrazine. The results of the test varied between effective and ineffective inhibition values, as described in the manuscript.

**Key words:** Azo dye, Antioxidant effectiveness, 3-aminophenol, 2,4,6-trihydroxyacetophenone, Thermogravimetric analysis.

## Introduction

The first theory of coordination compounds was developed by Swiss chemist Alfred Werner (1866–1919)<sup>1</sup>. Coordination compounds are one of the most important and challenging areas in modern inorganic chemistry<sup>2</sup>. A better understanding of chemical bonding and molecular structure has provided insight into how these compounds function as integral components of a biological system.

Derivatives of azo dyes showed diversity of activity in bio-efficacy, including the anti-inflammatory<sup>3</sup>, antiviral<sup>4</sup>, antimicrobial, and anticancer activities<sup>5</sup>. Furthermore, multidentate sulfa azo dye ligands displayed an important role in forming sensibly stable complexes with most of the transition metals<sup>6</sup>. Oxygen, nitrogen, and sulfur donor ligands have been attracted featured attentiveness because of their

mixed soft-hard donor properties beside multilateral coordination characters, and their excellent biological activity, i.e. toxicity towards the growth of bacteria, anticancer activity and other biochemical characteristics<sup>7</sup>. Furthermore, di- and poly-nuclear transition metal chelates have been received great interest due to their marvelous spectroscopic and magnetic characteristics<sup>8</sup>, their attractive uses in the field of material sciences<sup>9</sup>, and remarkable applications in important biological systems<sup>10-12</sup>. The chromophoric azo group  $-N=N-$  gives amazing properties for azo dyes such as the absorption in visible region, chromic and photochromic properties bond to ion metals, binding to DNA. Azo dyes and their complexes play important role in the dye-sensitized solar cells (DSSCs) as sensitizers<sup>13</sup>. Azo-dyes are considered as a class of organic compounds which have at least one conjugated chromophoric azo linkage ( $-N=N-$ ) associated with one or more aromatic or heterocyclic moieties in their structures.

## Materials and Methods

All the starting materials, chemicals and solvents for the prepared compounds were of analytical grade. Abs. EtOH, MeOH, DMSO and other solvents were of high purity and supplied by Merck Co., Fluka Co. and Sigma-Aldrich Co., and metal salts [ $FeCl_3$ ,  $CrCl_3 \cdot 6H_2O$ ,  $RhCl_3 \cdot 3H_2O$ ,  $RuCl_3 \cdot 3H_2O$ ,  $(NH_4)_2MoO_4$  and  $CoCl_2 \cdot 6H_2O$ ,] were of high purity and supplied by Sigma-Aldrich Co. and BDH Co., The melting point of the prepared ligand and complexes were measured by a Stuart electrothermal melting point apparatus. The elemental micro-analysis (C H N), to search using the EA 3000 single. LC-MSQP50A(E30ev) Shimadzu device. Infrared spectra were measured with a device (Shimadzu-8000S). The UV-1800 Shimadzu Spectrophotometer was used to record the UV-visible absorption. Molar electrical conductivity measurements were carried out using BC3020 Professional Bench Top Conductivity device. All earlier types of thermal analysis employed Perkin-Elmer Pyris Diamond DSC/TGA.

### Synthesis of Ligand 1-(2,4,6-trihydroxy-3-((3-hydroxyphenyl) diazenyl) phenyl) ethan-1-one.

The synthesis process of the ligand is carried out in two steps, Scheme.1, first step is the preparation of diazonium salt at which (1g, 0.01mol) from 2,4,6-trihydroxyacetophenone dissolved in round-bottomed flask 250 cm<sup>3</sup> in size with the

They can be classified either according to colour aspects (application in dye works) or by chemical guidelines (characteristic chemical groups). Azo-dyes derived from aromatic amines and their metal complexes have widespread applications in various fields. They are the subject of many research works because of their applications as textile dyes, pharmaceutical materials and indicators. Furthermore, they have important roles in food and Analytical Chemistry<sup>14</sup>. This research aims to prepare novel complexes of the metal ions ( $Cr^{+3}$ ,  $Co^{+2}$ ,  $Rh^{+3}$ ,  $Fe^{+3}$ ,  $Mo^{+6}$ , and  $Ru^{+3}$ ) using the azo ligand H<sub>4</sub>L. Thereafter, characterization by spectroscopic analysis, thermal stability, and thermal decomposition will be studied using DSC and TGA curves, and the antioxidant activity of these compounds will be assessed against the DPPH radical and compared with D-ascorbic acid as a reference.

mixture of (3 cm<sup>3</sup> Hydrochloric acid HCl 37% with 35 cm<sup>3</sup> distilled water DW) then the prepared mixture was cooled between 0-5 °C. After that, the solution of (1g, 0.01mol) sodium nitrate  $NaNO_2$  that dissolved in 30 cm<sup>3</sup> of distilled water was added to the last mixture dropwise with continuous stirring, monitoring of temperature as it must not rise more than 5 °C, for 30 minutes, in the next step, the solution was left for 30 minutes resulting in diazonium salt as a product of the first step. This was followed by diazotization coupling reaction between diazonium salt of 3-aminophenol and the solution of (1.5g, 0.004 mol.) (2,4,6-trihydroxyacetophenone) dissolved in 50 cm<sup>3</sup> absolute ethanol and 15 cm<sup>3</sup> of 10% sodium hydroxide NaOH with cooling and continuous stirring during this process observed the precipitates were obtained in different colors. Fig. 1 shows both <sup>1</sup>H- & <sup>13</sup>C-NMR data for the ligand. Proton NMR demonstrates the next chemical shifts in ppm: 2.6δppm (3H, Singlet), 7.5-8.0δppm (5H, multiplate) and 9.75-9.98δppm (4H, doublet). Corresponding to protons of methyl group of ketone, Ar-H protons and protons of phenolic groups respectively. On the other hand, carbon NMR spectrum which tested using chloroform as solvent demonstrates the next peaks: 178.8 (C1), 137.4 (C2), 165 (C3), 156.2 (C4), 174.0 (C5), 155 (C6), 127.0 (C7), 182.0 (C8), 106.5 (C9), 190.0 (C10), 119.0 (C11), 170.0 (C12), 195.0 (C13), 49.9 (C14)<sup>15, 16</sup>.

### Preparation of Metallic Metal ions Complexes

Following the same approach used in rhodium complex synthesis, the complexes of the next metal salts. (0.4 mmol)  $[\text{CrCl}_3 \cdot 6\text{H}_2\text{O}]$  (0.1g, 0.6 mmol),  $(\text{CoCl}_2 \cdot 6\text{H}_2\text{O})$  (0.1g, 0.8 mmol),  $(\text{FeCl}_3)$  (0.1g, 0.6 mmol),  $(\text{RhCl}_3 \cdot 3\text{H}_2\text{O})$ , (0.1g, 0.4 mmol),  $(\text{RuCl}_3 \cdot 3\text{H}_2\text{O})$ , (0.1g, 0.4 mmol) and  $(\text{NH}_4)_2\text{MoO}_4$ , (0.1g, 0.5 mmol) were prepared. To dissolve the salts,  $10 \text{ cm}^3$  of water is used. Next, drop by drop,  $15 \text{ cm}^3$  of azo ligand ( $\text{H}_4\text{L}$ ) weighing 0.1g and 0.4mmol is added to the solution. The mixture is then heated and refluxed for 2 hours at a temperature of up to  $40^\circ\text{C}$ . After that, any un reacted components are removed by briefly immersing them in hot ethanol. The solid complexes formed are then separated, collected, dried and weighed. The formation of the

metal complexes is shown in Scheme.1. Fig. 2 shows both  $^1\text{H}$ -&  $^{13}\text{C}$ -NMR data for the Rh-complex.  $^1\text{H}$ -NMR demonstrates the next chemical shifts in ppm: 2.32  $\delta\text{ppm}$  (3H, Singlet), 7.01- 7.58  $\delta\text{ppm}$  (5H, multiplate) and 9.91-10.11  $\delta\text{ppm}$  (2H, doublet). Corresponding to protons of methyl group of ketone, Ar-H protons and protons of phenolic groups respectively and 3.32  $\delta\text{ppm}$  (Singlet) for attributed to the DHO. On the other hand,  $^{13}\text{C}$ -NMR spectrum which tested using chloroform as solvent demonstrates the next peaks: 189.88 (C1), 140.74 (C2), 165.44 (C3), 169.11 (C4), 151.41 (C5), 127.41 (C6), 127.51 (C7), 181.27 (C8), 105.84 (C9), 172.05 (C10), 119.01 (C11), 178.62 (C12), 200.41 (C13), 30.51 (C14)<sup>15,16</sup>.

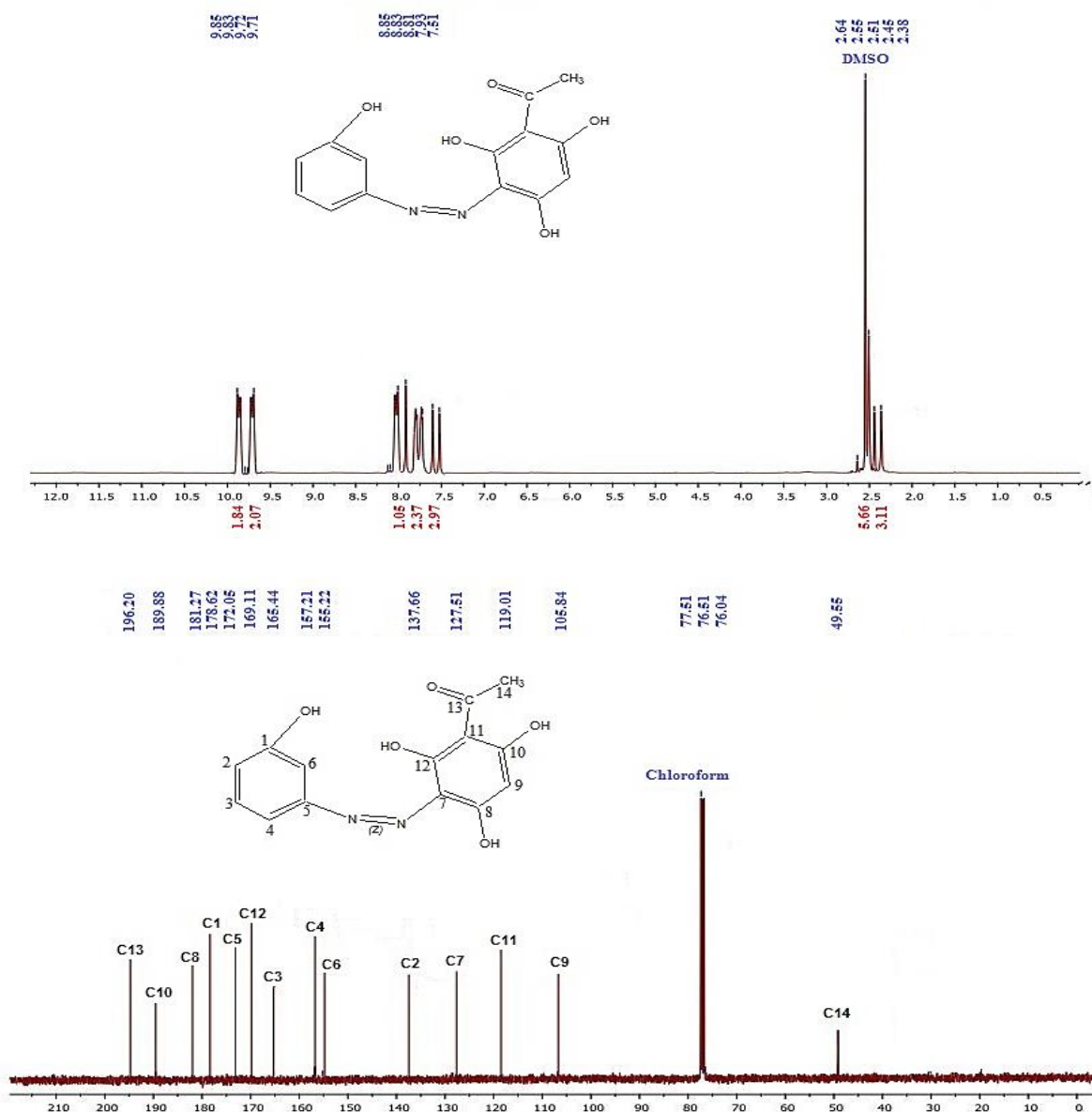


Figure 1.  $^1\text{H}$ -&  $^{13}\text{C}$ -NMR spectra of ligand (H<sub>4</sub>L)

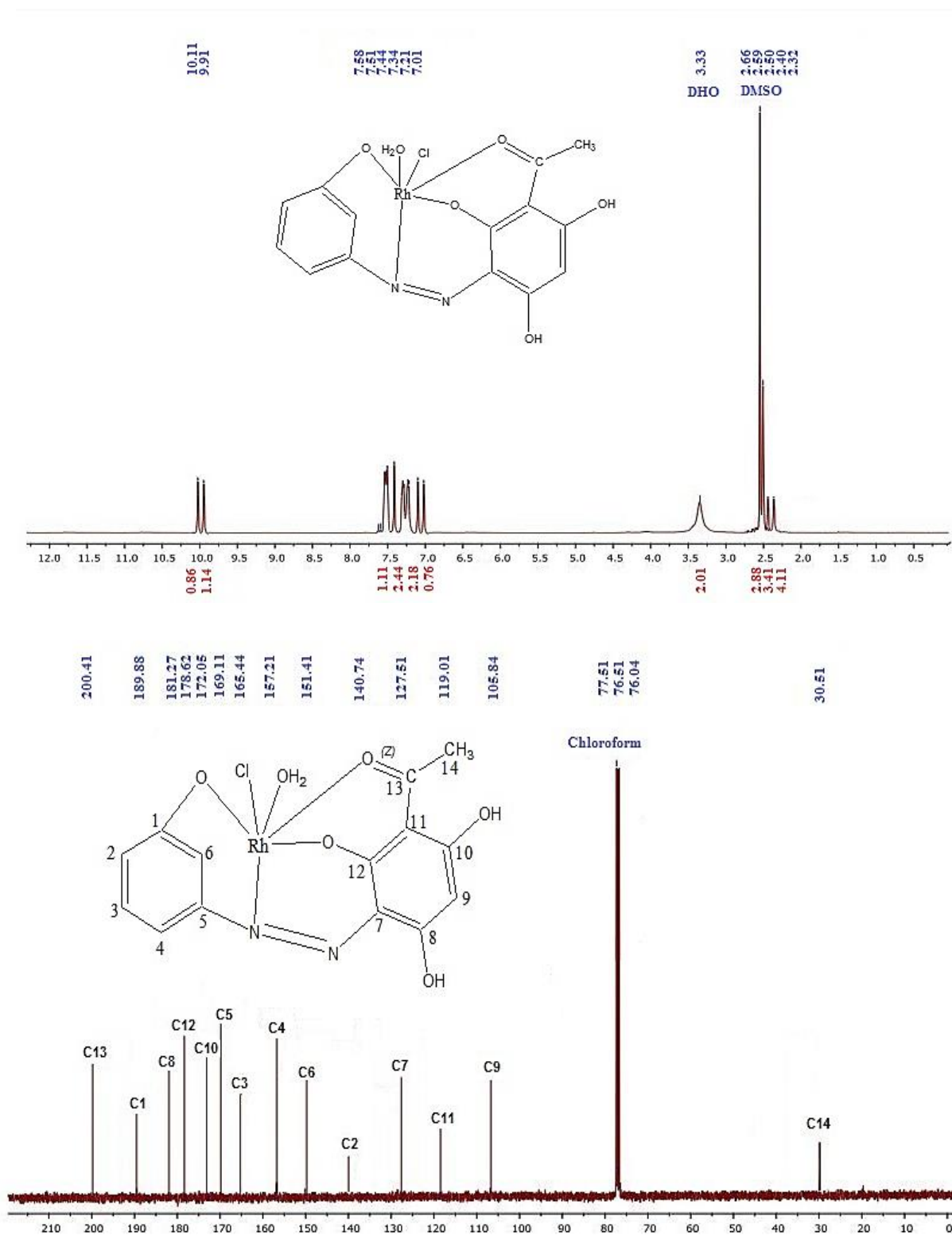
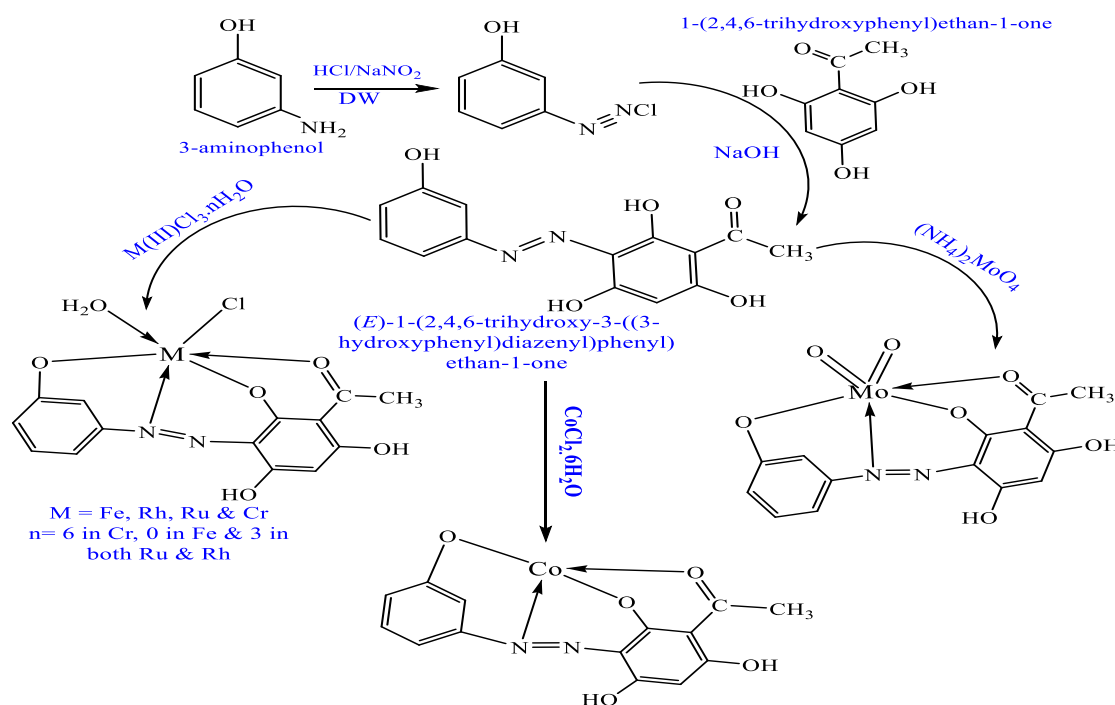


Figure 2.  $^1\text{H}$ -&  $^{13}\text{C}$ -NMR spectra of Rh-complex



**Scheme 1. Synthesis of ligand (H<sub>4</sub>L) and its complexes.**

## Results and discussion

Table.1 shows the comparison between the estimated and theoretical results of the percentage of each element involved in synthesized complexes, as well as the chloride involvement and metal ratio. The

estimated results were obtained both technically and theoretically, and were found to be in good agreement with each other.

**Table 1. Colours, yields, elemental analyses, and molar conductance values**

Compound (M. wt)	Elemental microanalysis % found (calc.)					Yield %	m.p°C	Colour
	C	H	N	M	Cl			
<b>C<sub>14</sub>H<sub>12</sub>N<sub>2</sub>O<sub>5</sub></b> <b>288.26</b>	57.89 (58.33)	4.67 (4.20)	10.11 (9.72)	-	-	50	146-148	Brown
<b>C<sub>14</sub>H<sub>12</sub>N<sub>2</sub>O<sub>6</sub>ClCr</b> <b>391.70</b>	41.78 (42.93)	4.02 (3.09)	8.07 (7.15)	12.34 (13.27)	10.00 (9.05)	68	>300	Brown
<b>C<sub>14</sub>H<sub>12</sub>N<sub>2</sub>O<sub>6</sub>ClFe</b> <b>395.55</b>	41.14 (42.51)	2.97 (3.06)	8.11 (7.08)	13.31 (14.12)	9.54 (8.96)	74	184-186	Dark brown
<b>C<sub>14</sub>H<sub>10</sub>N<sub>2</sub>O<sub>5</sub>Co</b> <b>345.17</b>	47.88 (48.71)	3.33 (2.92)	7.91 (8.12)	18.01 (17.07)	nil	69	240 D	Reddish brown
<b>C<sub>14</sub>H<sub>10</sub>N<sub>2</sub>O<sub>7</sub>Mo</b> <b>414.18</b>	40.6 (41.12)	2.43 (3.01)	6.76 (7.75)	23.16 (24.01)	-	71	193-195	Reddish brown
<b>C<sub>14</sub>H<sub>12</sub>N<sub>2</sub>O<sub>6</sub>ClRh</b> <b>442.04</b>	38.01 (37.99)	2.55 (2.73)	7.21 (6.33)	-	7.49 (8.01)	60	249 D	Dark brown
<b>C<sub>14</sub>H<sub>12</sub>N<sub>2</sub>O<sub>6</sub>ClRu</b> <b>440.78</b>	38.11 (38.15)	3.08 (2.74)	7.33 (6.36)	-	9.00 (8.04)	89	193-195	Dark brown

D=decompose

## FT-IR Spectroscopy

FT-IR spectroscopy can determine the formation of new complexes by comparing the spectra of the complexes with the spectrum of the ligand. The modifications observed in the spectra of

the complexes may include changes in the shape or intensities of the main bands, or a shift in their wavelengths towards lower or higher readings. In Fig. 3, the (H<sub>4</sub>L) ligand exhibited the following stretching absorption bands: A weak to strong band

at 3120  $\text{cm}^{-1}$  for the vibration of C-H aromatic group, a weak band at 2912  $\text{cm}^{-1}$  belonging to C-H aliphatic group, a moderate, sharp band at 1631  $\text{cm}^{-1}$  for the vibrational mode of carbonyl group (C=O) and bending absorption band for  $\text{CH}_3$  group at 1400  $\text{cm}^{-1}$ . Moreover, a unique band at 1463  $\text{cm}^{-1}$  was observed, which was not present in the starting materials. This band may be attributed to the vibrational mode of azo-group (N=N) and is considered strong evidence of azo formation<sup>17</sup>. The cobalt complex shows the following absorption peaks: a weak stretching absorption band of the C-H aromatic group at 3000  $\text{cm}^{-1}$ , overlapped with the broad band of the phenolic group (O-H) appearing at 3400  $\text{cm}^{-1}$ . Additionally, we can clearly see the stretching weak band of the C-H aliphatic group at 2950  $\text{cm}^{-1}$ . The change in the intensity of the azo-band that appeared at 1462  $\text{cm}^{-1}$  may have happened due to the coordinative behavior with the metal ion through this group. The strong evidence that supports this fact is the appearance of a new band called M-N band at 497  $\text{cm}^{-1}$ . The shifting in the location of the carbonyl absorption band compared to its location in the free ligand to be appeared at 1612  $\text{cm}^{-1}$  is also a good indication that proves the coordinative behavior through this group. Finally, the appearance of the Co-O band at 430  $\text{cm}^{-1}$  also proves the coordination through carbonyl and carbinol groups<sup>18</sup>. The iron complex exhibits various stretching absorption bands, including a broad band of phenolic group O-H, C-H aromatic group that overlaps with O-H and aqua group, C-H aliphatic group, azo-group (N=N), carbonyl group C=O, and carbinol group C-O. These bands were detected at 3473  $\text{cm}^{-1}$ , 3178  $\text{cm}^{-1}$ , 2926  $\text{cm}^{-1}$ , 1452  $\text{cm}^{-1}$ , 1598  $\text{cm}^{-1}$ , and 1307  $\text{cm}^{-1}$ , respectively. The same bands were observed in the

ligand with some modifications, such as shifting and changing in their intensities due to the interaction with the metal ion. Additionally, there are new bands, including the aqua band  $\text{H}_2\text{O}$  (3415, 1620 and 682  $\text{cm}^{-1}$ ), Fe-N (500  $\text{cm}^{-1}$ ), and Fe-O (466  $\text{cm}^{-1}$ )<sup>19</sup>, as displayed in Table 2. The molybdenum complex exhibits several stretching absorption bands, including a broad band of phenolic group O-H, C-H aromatic group that overlaps with O-H, C-H aliphatic group, azo-group (N=N), carbonyl group C=O, and carbinol group C-O. These bands were detected at 3413  $\text{cm}^{-1}$ , 3178  $\text{cm}^{-1}$ , 2921  $\text{cm}^{-1}$ , 1452  $\text{cm}^{-1}$ , 1598  $\text{cm}^{-1}$ , and 1307  $\text{cm}^{-1}$ , respectively. These same bands are observed in the ligand, but with some modifications such as shifting and changing in their intensities due to the interaction with metal ion. There are also new bands to consider, which are Mo-N and Mo-O<sup>20</sup>, as displayed in Table 2. Fig. 4 of the rhodium complex, displays the next stretching absorption bands: (weak band of phenolic group O-H, C-H aromatic group that overlapped with O-H and aqua groups, C-H aliphatic group, azo-group (N=N), carbonyl group C=O and carbinol group C-O). Those bands were detected at 3749  $\text{cm}^{-1}$ , 3010  $\text{cm}^{-1}$ , 2922  $\text{cm}^{-1}$ , 1462  $\text{cm}^{-1}$ , 1620  $\text{cm}^{-1}$  and 1257  $\text{cm}^{-1}$  respectively. Those bands are the same bands that observed in ligand with some modifications such as shifting and changing in their intensities due to the interaction with metal ion. Other bands are considered new bands, those are: aqua band  $\text{H}_2\text{O}$ , Rh-N and Rh-O<sup>21</sup> as displayed in Table 2, for ruthenium complex, displays the same bands that detected in previous complex (Rh-complex) with some variations such as shifting and intensity changing as displayed in Table 2.

**Table 2. FT-IR spectral data for ligand and complexes**

Compounds	(H <sub>2</sub> O) aqua	(OH) phenolic	(C-H) aromatic	(C-H) aliphatic	(N=N)	C-O	(C=O)	M-N (M-O)
C <sub>14</sub> H <sub>12</sub> N <sub>2</sub> O <sub>5</sub> (H <sub>4</sub> L)	-	3580	3120	2912	1463	1282	1631	--
C <sub>14</sub> H <sub>10</sub> N <sub>2</sub> O <sub>5</sub> Co	-	3400	3000	2950	1462	1305	1612	497 (430)
C <sub>14</sub> H <sub>12</sub> N <sub>2</sub> O <sub>6</sub> ClFe	3415 1620 682	3473	3178	2926	1400 1452	1307	1598	500 (466)
C <sub>14</sub> H <sub>10</sub> N <sub>2</sub> O <sub>7</sub> Mo	-	3413	3178	2921	1400 1452	1307	1598	523 (410)
C <sub>14</sub> H <sub>12</sub> N <sub>2</sub> O <sub>6</sub> ClRh	3280 1699 771 630	3749	3010	2922	1404 1462	1257	1620	493 (450)
C <sub>14</sub> H <sub>12</sub> N <sub>2</sub> O <sub>6</sub> ClRu	3425 1617 760	3757	3100 overlapped	2926	1404 1463	1120	1612	493 (478)

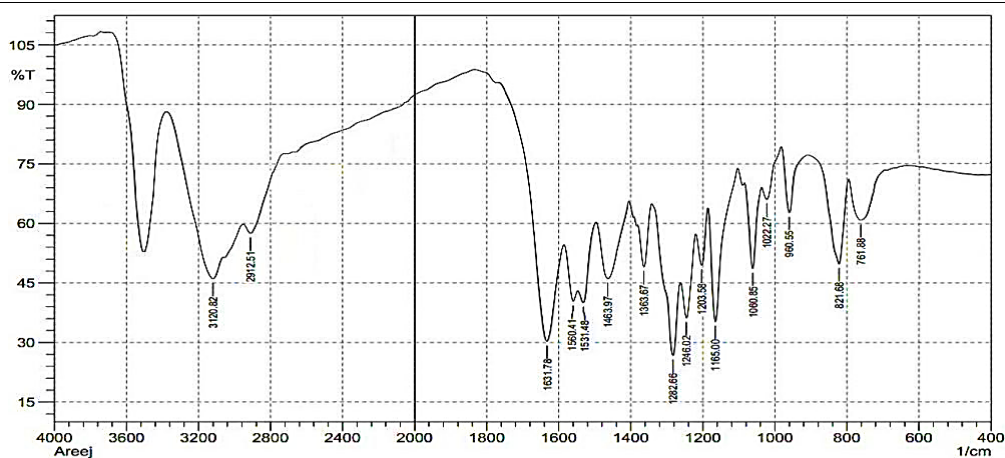


Figure 3. FT-IR spectrum for ligand (H<sub>4</sub>L)

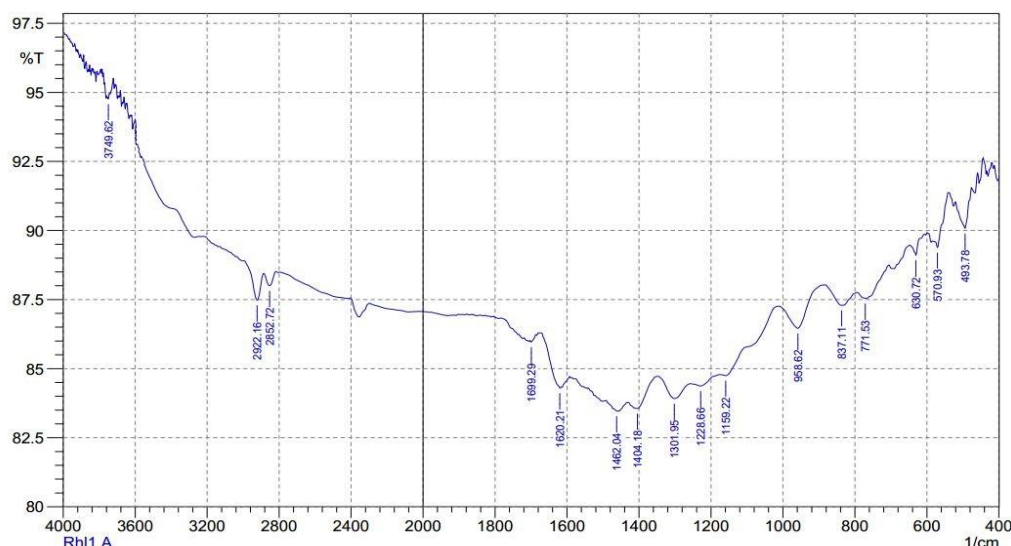


Figure 4. FT-IR spectrum for Rh-complex

### The ligand and its complexes are studied by UV-Vis, molar conductivity and magnetic susceptibility

The UV-vis spectrum of (H<sub>4</sub>L) ligand Fig. 5 shows a moderately broad absorption band at 300 nm, 33333 cm<sup>-1</sup>) corresponding to ( $\pi \rightarrow \pi^*$ ) electronic transition, and another broad band at 391 nm, 25575 cm<sup>-1</sup>) corresponding to  $n \rightarrow \pi^*$  electronic transition<sup>22</sup>. Fig. 6 demonstrates the spectrum of chromium complex and the next transitions: ( $\pi \rightarrow \pi^*$ ,  $n \rightarrow \pi^*$  and C. T L $\rightarrow$ M) at (210 nm, 47619cm<sup>-1</sup>), (290 nm, 34482 cm<sup>-1</sup>) and (387 nm, 25839 cm<sup>-1</sup>) respectively, the transitions of ligand with some shifting in their wavelengths because of coordination with metal. In addition to d-d transitions at visible region (600 nm, 16666 cm<sup>-1</sup>) and (790 nm, 12658 cm<sup>-1</sup>) belonging to  ${}^4A_{2g} \rightarrow {}^4T_{2g} (F)$  and  ${}^4A_{2g} \rightarrow {}^4T_{1g} (F)$  respectively.  $\mu_{\text{eff}} =$

3.89 which is an indicative of an Octahedral geometry<sup>23</sup>. Ultra-violet-visible spectrum of iron complex in Fig. 7, shows two transitions in UV-region at 290 nm, 34482 cm<sup>-1</sup> and 310 nm, 32258 cm<sup>-1</sup> belonging to  $\pi \rightarrow \pi^*$  and  $n \rightarrow \pi^*$  transitions respectively<sup>23</sup>. In addition to d-d transitions in visible region at 413 nm, 24213 cm<sup>-1</sup>, 645 nm, 15503 cm<sup>-1</sup> and (800 nm, 12500 cm<sup>-1</sup>) corresponding to  $n \rightarrow \pi^* + C. T (M \rightarrow L)$ ,  ${}^6A_{1g} \rightarrow {}^4A_{1g}, E_g$  and  ${}^6A_{1g} \rightarrow {}^4T_{2g}$  respectively  $\mu_{\text{eff}} = 5.69$  which is an indicative of an Octahedral geometry. Ultra-violet-visible spectrum of cobalt complex in Fig.8, demonstrates the next peaks at ultra-violet region: (250 nm, 40000 cm<sup>-1</sup>) and (300 nm, 33333 cm<sup>-1</sup>) belonging to  $\pi \rightarrow \pi^*$  and  $n \rightarrow \pi^*$  transitions respectively. And next peaks at visible region: (410 nm, 24390 cm<sup>-1</sup>) and (630 nm, 15873 cm<sup>-1</sup>) corresponding to C. T (M $\rightarrow$ L) and

${}^4A_2 \rightarrow {}^4T_1(F)$  transitions respectively  $\mu_{\text{eff}} = 3.88$  which is an indicative of a Tetrahedral geometry<sup>24</sup>. Ultraviolet-visible spectrum of Rhodium complex shows the following transitions: ( $\pi \rightarrow \pi^*$ ,  $n \rightarrow \pi$ , C.T  $M \rightarrow L$ ,  ${}^1A_1g \rightarrow {}^1T_2g$  and  ${}^1A_1g \rightarrow {}^1T_1g$ ) at (280 nm,  $35714 \text{ cm}^{-1}$ ), (300 nm,  $33333 \text{ cm}^{-1}$ ), (410 nm,  $24390 \text{ cm}^{-1}$ ) (630,  $15873$ ), (780,  $12820$ ) respectively. Which is an indicative of an Octahedral geometry. The UV-Vis spectrum of molybdenum complex displays the next transitions: at ultra-violet region ( $\pi \rightarrow \pi^*$  and  $n \rightarrow \pi^*$ ) transitions corresponding to (280 nm,  $35714 \text{ cm}^{-1}$  and 315 nm,  $31746 \text{ cm}^{-1}$ ) respectively. In addition to single transition at visible region at (425 nm,  $23529 \text{ cm}^{-1}$ ) attributed to C.TL  $\rightarrow M$  transition. Which is an indicative of an Octahedral geometry. Ultraviolet-visible spectrum of ruthenium complex shows the following transitions: ( $\pi \rightarrow \pi^*$ ,  $n \rightarrow \pi$ ,  ${}^1A_1g \rightarrow {}^1T_1g$  and  ${}^1A_1g \rightarrow {}^1T_2g$ ) at (290 nm,  $34482 \text{ cm}^{-1}$ ), (300 nm,  $33333 \text{ cm}^{-1}$ ), (420 nm,  $23809 \text{ cm}^{-1}$ ) and (500 nm,  $20000 \text{ cm}^{-1}$ ) respectively.  $\mu_{\text{eff}} = 1.71$ , which is an indicative of an Octahedral geometry<sup>25</sup>. All complexes exhibit the same absorption bands as those found in the ligand, located in the ultraviolet region. However, there are some modifications, including a shift in their absorption bands due to coordinative binding with metal ions. Furthermore, the spectra show new absorption peaks in the visible region, which belong to d-d transitions, as shown in Table 3. The molar conductivity of the synthesized complex solutions was measured by preparing  $1 \times 10^{-3} \text{ M}$  from the complexes in DMSO solvent at room temperature. It was found that all measurements shown in Table 3 were consistent with the suggested structural formula of all complexes, indicating that all complexes are non-electrolytes and confirming the geometries of the obtained complexes. Magnetic susceptibility measurements have been widely used in the diagnosis and study of complex transition metals. The most important aspect in this field relates to the effects resulting from the partially filled outer casings with electrons. Magnetic measurements provide information about the compound in terms of the electronic arrangement and the oxidation state of the transition metal atoms. The number of lone electrons of a transition metal ion indicates the state of the spin of the studied complex, whether it is spinning low or high<sup>26</sup>.

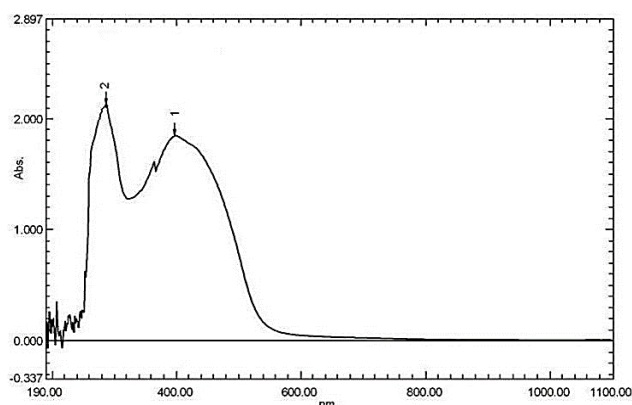


Figure 5. UV-vis spectrum of Ligand (H<sub>4</sub>L)

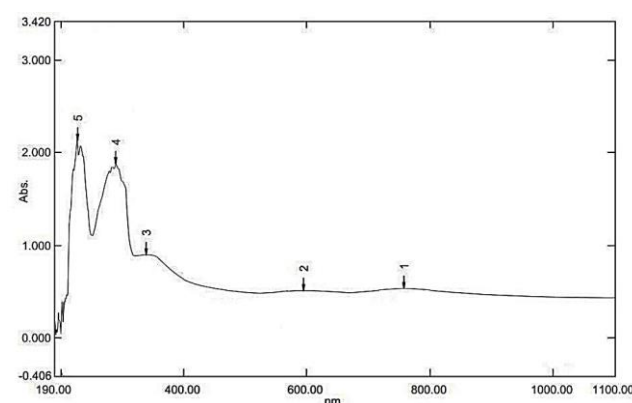


Figure 6. UV-Vis spectrum of Cr-complex

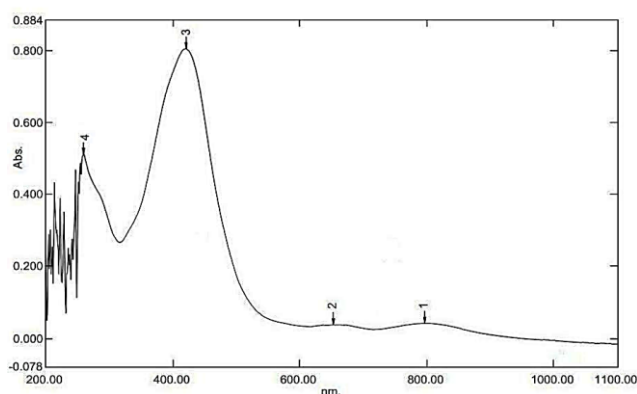


Figure 7. UV-vis spectrum of Fe-complex

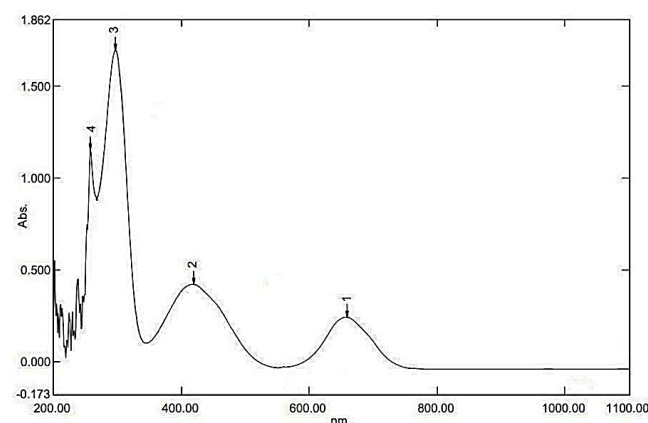


Figure 8. UV-vis spectrum of Co-complex

Table 3. Electronic spectral data of the compounds and magnetic moment

Compound	$\lambda_{\max}$ (nm)	$\nu_{\text{cm}^{-1}}$	ABS.	$\epsilon_{\text{max}} \text{ L mol}^{-1} \text{ cm}^{-1}$	$\Lambda_{\text{m}} \text{ cm}^2 \Omega^{-1} \text{ mol}^{-1}$	Assignment	$\mu_{\text{eff}}$ practical (theoretical)
$\text{C}_{14}\text{H}_{12}\text{N}_2\text{O}_5$ ( $\text{H}_4\text{L}$ )	300	33333	2.090	2090		$\pi \rightarrow \pi^*$	-
	391	25575	1.850	1850	--	$n \rightarrow \pi^*$	
	210	47619	2.000	2000		$\pi \rightarrow \pi^*$	
$\text{C}_{14}\text{H}_{12}\text{N}_2\text{O}_6\text{ClCr}$ Octahedral	290	34482	1.900	1900		$n \rightarrow \pi^*$	3.89
	387	25839	0.900	900.0	13	C.T (L $\rightarrow$ M)	(3.872)
	600	16666	0.600	600.0		${}^4\text{A}_{2g} \rightarrow {}^4\text{T}_{2g}(\text{F})$	
$\text{C}_{14}\text{H}_{12}\text{N}_2\text{O}_6\text{ClFe}$ Octahedral	790	12658	0.650	650.0		${}^4\text{A}_{2g} \rightarrow {}^4\text{T}_{1g}(\text{F})$	
	290	34482	0.570	570		$\pi \rightarrow \pi^*$	
	310	32258	0.400	400		$n \rightarrow \pi^*$	5.69
	413	24213	0.800	800	17	$n \rightarrow \pi^* + \text{C.T}$ (M $\rightarrow$ L)	(5.916)
$\text{C}_{14}\text{H}_{10}\text{N}_2\text{O}_5\text{Co}$ Tetrahedral	645	15503	0.050	50		${}^6\text{A}_{1g} \rightarrow {}^4\text{T}_{2g}$	
	800	12500	0.050	50		${}^6\text{A}_{1g} \rightarrow {}^4\text{T}_{2g}$	
	250	40000	1.200	1200		$\pi \rightarrow \pi^*$	
$\text{C}_{14}\text{H}_{12}\text{N}_2\text{O}_6\text{ClRh}$ (Octahedral)	300	33333	1.570	1570	10	$n \rightarrow \pi^*$	3.88
	410	24390	0.400	400		C.T (M $\rightarrow$ L)	(3.872)
	630	15873	0.200	200		${}^4\text{A}_2 \rightarrow {}^4\text{T}_1(\text{F})$	
	280	35714	0.400	400		$\pi \rightarrow \pi^*$	
$\text{C}_{14}\text{H}_{10}\text{N}_2\text{O}_7\text{Mo}$ (Octahedral)	300	33333	0.550	550		$n \rightarrow \pi^*$	
	410	24390	0.680	680	6	C.T M $\rightarrow$ L	Diamagnet ic
	630	15873	0.050	50.0		${}^1\text{A}_{1g} \rightarrow {}^1\text{T}_{2g}$	(0)
$\text{C}_{14}\text{H}_{12}\text{N}_2\text{O}_6\text{ClRu}$ (Octahedral)	780	12820	0.060	60.0		${}^1\text{A}_{1g} \rightarrow {}^1\text{T}_{1g}$	
	280	35714	2.200	2200		$\pi \rightarrow \pi^*$	Diamagnet ic
	315	31746	1.800	1800	18	$n \rightarrow \pi^*$	(0)
$\text{C}_{14}\text{H}_{12}\text{N}_2\text{O}_6\text{ClRu}$ (Octahedral)	425	23529	0.600	600		C.TL $\rightarrow$ M	(0)
	290	34482	1.980	1980		$\pi \rightarrow \pi^*$	1.71
	300	33333	2.000	2000	9	$n \rightarrow \pi^*$	(1.732)
	420	23809	0.700	700		${}^1\text{A}_{1g} \rightarrow {}^1\text{T}_{1g}$	
	500	20000	0.600	600		${}^1\text{A}_{1g} \rightarrow {}^1\text{T}_{2g}$	

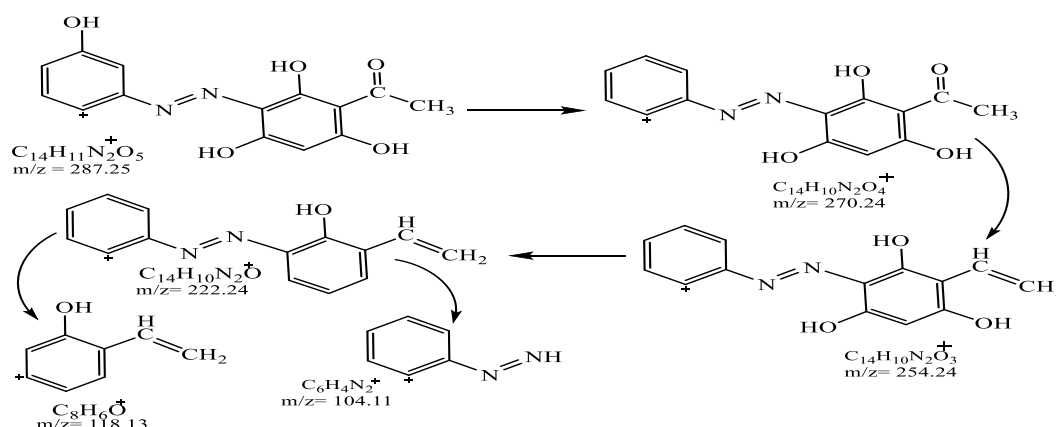
### LC-Mass Spectra for Ligand ( $\text{H}_4\text{L}$ ) and Some Complexes:

LC-Mass spectrum testing is one of the most crucial methods for characterizing the ligand ( $\text{H}_4\text{L}$ ) and some products. It supplements other methods that estimate the molecular weight of the chemical. The fragmentation pattern and the extract mass for each pattern are shown in Scheme 2 to provide mass information for the ligand. The fragment's molecular ion peak  $[\text{M}]^+$  is easily visible, such as  $\text{C}_{14}\text{H}_{11}\text{N}_2\text{O}_5^+$  with a relative abundance of about 9% in Fig. 9. Other abundances are also present for the rest of the peaks:  $\text{C}_{14}\text{H}_{10}\text{N}_2\text{O}_4^+$ ,  $\text{C}_{14}\text{H}_{10}\text{N}_2\text{O}_3^+$ ,  $\text{C}_{14}\text{H}_{10}\text{N}_2\text{O}^+$ ,  $\text{C}_8\text{H}_6\text{O}^+$  and  $\text{C}_6\text{H}_4\text{N}_2^+$  corresponded the next abundances :270.24 m/z, 254.24 m/z, 222.24 m/z, 118.13 m/z and 104.11 m/z respectively<sup>27</sup>. For molybdenum complex, Fig. 10 and Scheme 2, we can

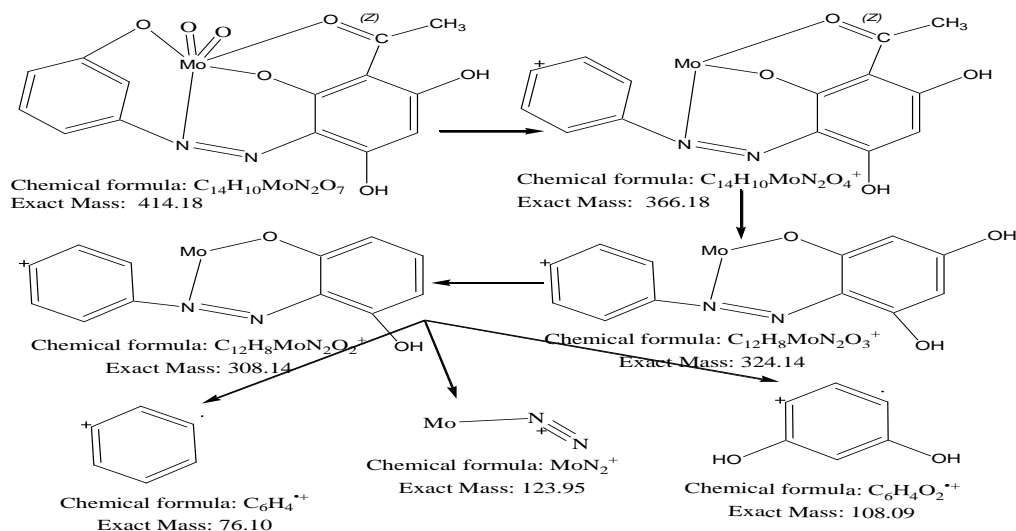
also detect the molecular ion peak ( $\text{M}^+$ ) at 414 m/z with relative abundance 10% and next pattern:  $\text{C}_{14}\text{H}_{10}\text{MoN}_2\text{O}_4$ ,  $\text{C}_{12}\text{H}_8\text{MoN}_2\text{O}_3$ ,  $\text{C}_{12}\text{H}_8\text{MoN}_2\text{O}_2$ ,  $\text{MoN}_2$ ,  $\text{C}_6\text{H}_4\text{O}_2$ , and  $\text{C}_6\text{H}_4$  which corresponded to: 366.18m/z, 324.14m/z, 308.14m/z, 223.15m/z, 123.95m/z, 76.10m/z respectively, corresponded the next abundances: 28%, 50%, 65%, 19%, 55%, 82%, 85% respectively. For cobalt complex in Fig. 11 and Scheme. 4, we can also detect the molecular ion peak ( $\text{M}^+$ ) at 345.21 m/z with relative abundance 10% and next pattern:  $\text{C}_{14}\text{H}_9\text{CoN}_2\text{O}_4^+$ ,  $\text{C}_{14}\text{H}_9\text{CoN}_2\text{O}_3^+$ ,  $\text{C}_6\text{H}_4\text{CoO}^+$ ,  $\text{C}_6\text{H}_4\text{N}_2\text{O}_2^+$ ,  $\text{C}_6\text{H}_4\text{CoO}$  which corresponded to 328.17m/z, 286.13m/z, 312.17m/z, 136.11m/z, 151.03 m/z respectively, corresponded the next abundances :28%, 47%, 68%, 46%, 80% respectively. For Rhodium complex, Scheme 5, we can also detect the molecular ion peak ( $\text{M}^+$ ) at

442m/z with relative abundance 25% and next pattern:  $C_{14}H_{10}ClRhN_2O_5^+$ ,  $C_{14}H_{10}RhN_2O_4^+$ ,  $C_{12}H_8RhN_2O_3^+$ ,  $C_{12}H_8RhN_2O_2^+$ ,  $C_6H_2O_2Rh$ ,  $C_6H_4N_2^+$  which corresponded to: 424.60m/z, 373.15m/z, 331.11m/z, 315.11m/z, 208.98m/z, 104.11m/z respectively, corresponded the next abundances :45%, 62%, 36%, 75%, 79%, 50% respectively<sup>28</sup>. For Chromium complex we can also detect the molecular ion peak ( $M^+$ ) at 391.84 m/z with relative abundance 24% and next pattern:

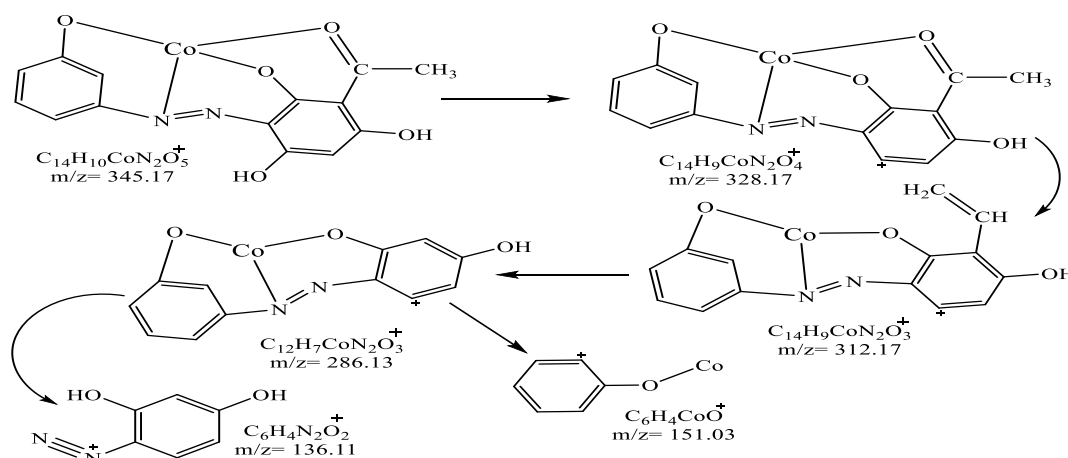
$C_{14}H_{10}ClCrN_2O_5^+$ ,  $C_{14}H_{10}CrN_2O_4^+$ ,  $C_{12}H_8CrN_2O_3^+$ ,  $C_{12}H_8CrN_2O_2^+$ ,  $C_6H_4O_2^+$ ,  $CrN_2^+$  Which corresponded to: 373.54 m/z, 322.17m/z, 280.14m/z, 264.31m/z, 108.41m/z, 79.68m/z, 76.22m/z respectively, corresponded the next abundances :55%, 42%, 32%, 75%, 50%, 62%, 88% respectively<sup>29</sup>. All the partitioning analogues and relative abundance for each analogue are illustrated in Table 4.



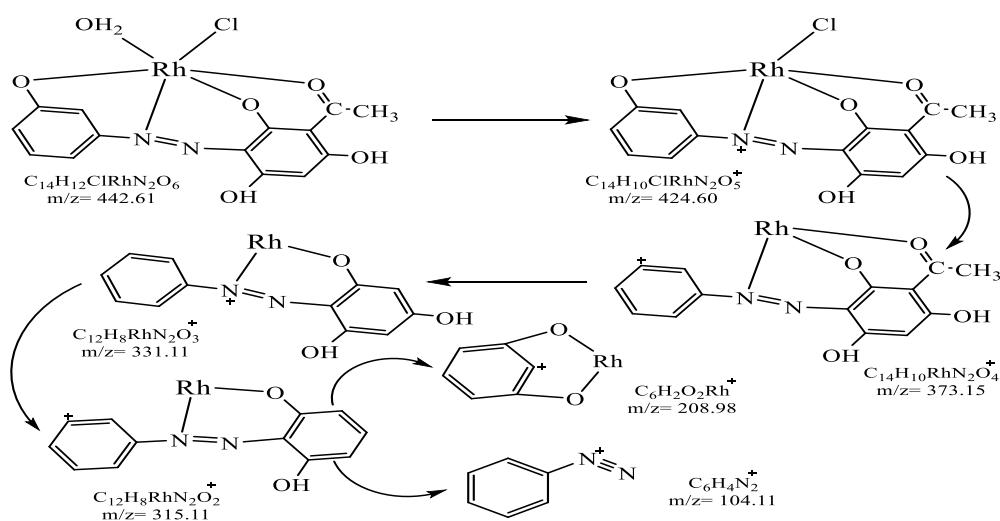
**Scheme 2. The proposed mass fragmentation pathways of ligand (H<sub>4</sub>L)**



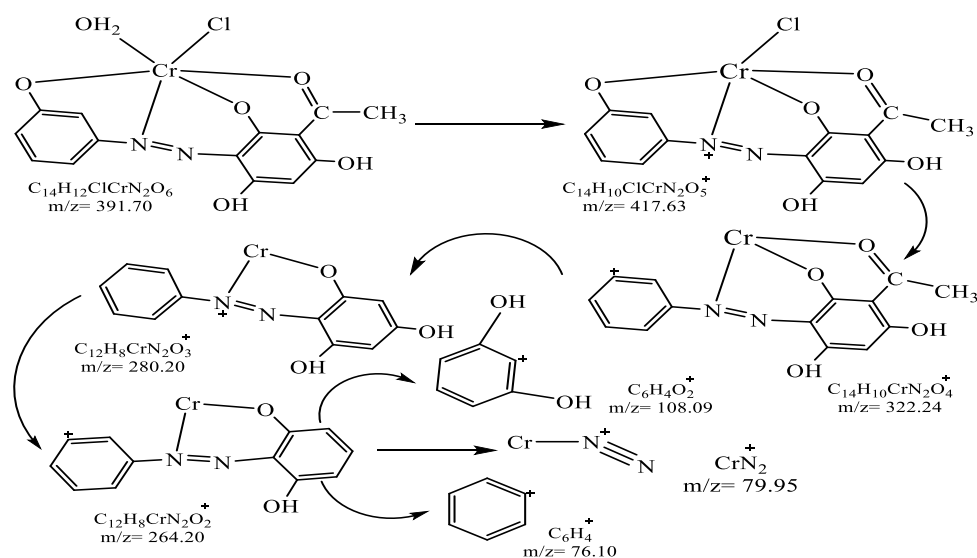
**Scheme 3. The proposed mass fragmentation pathways of Mo-complex**



**Scheme 4. The proposed mass fragmentation pathways of Co-complex**



**Scheme 5. The proposed mass fragmentation pathways of Rh-complex**



**Scheme 6. The proposed mass fragmentation pathways of Cr-complex**

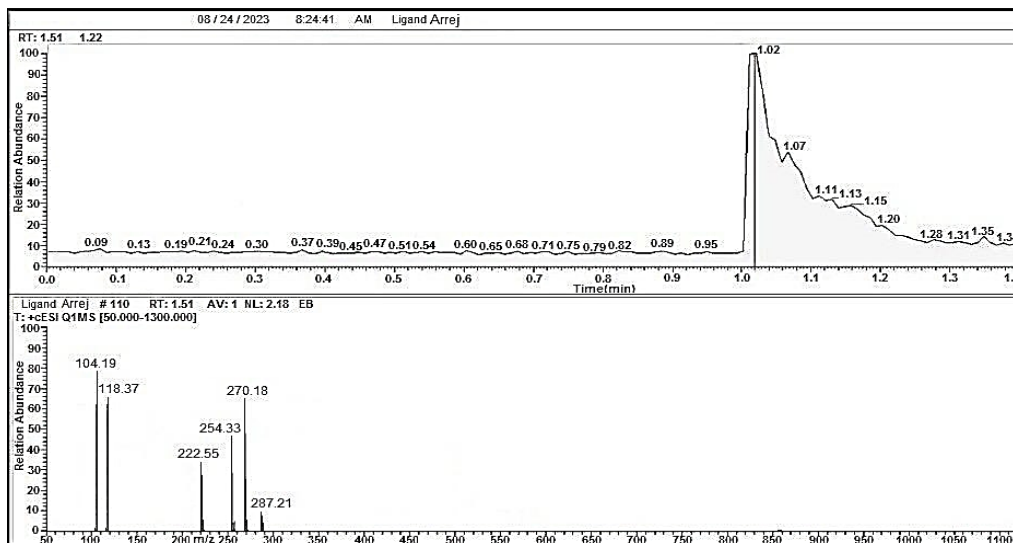


Figure 9. LC-Mass spectrum of ligand (H<sub>4</sub>L)

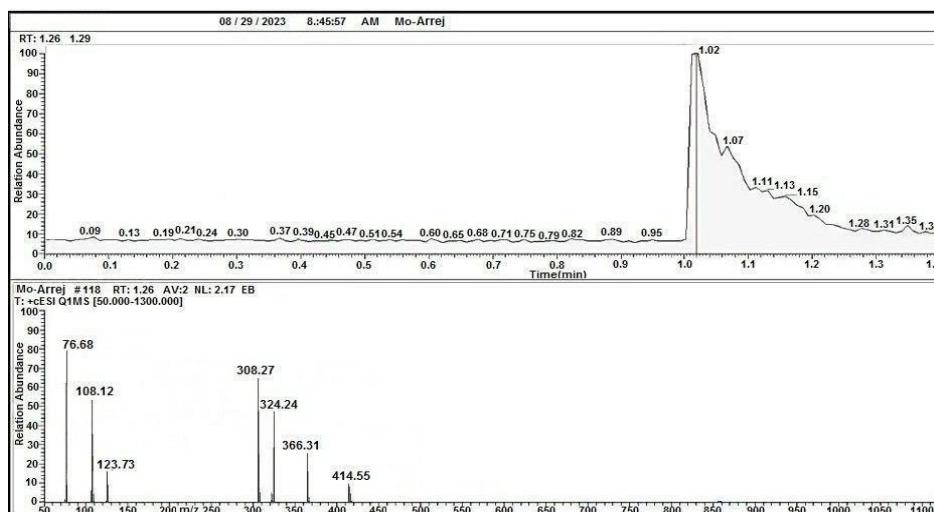


Figure 10. LC-Mass spectrum of molybdenum complex

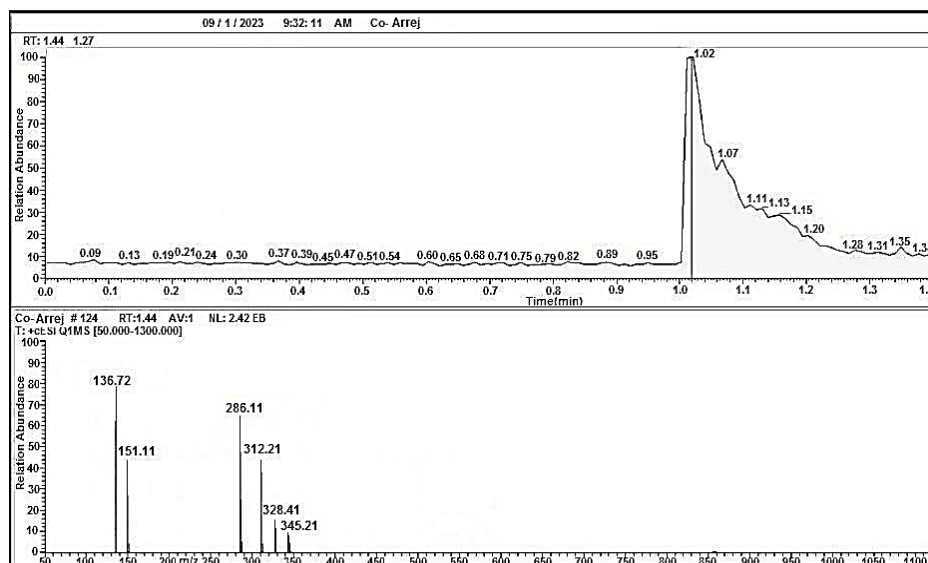


Figure 11. LC-Mass spectrum of cobalt complex

### Thermal Analysis Diagnosis:

DSC (differential scanning calorimetric) is a pyrolysis technique that helps to determine the amount of temperature absorbed and released during thermal changes in a substance. It is widely used in various fields such as minerals, organic compounds, pharmaceuticals, polymers, inorganic substances and food to determine their purity and stability.  $T_i/^\circ\text{C}$ ,  $T_f/^\circ\text{C}$  and heat amount  $\Delta H$  J/g enthalpy in units are measured for exothermic or endothermic reactions,  $\Delta S$  entropy a measure of the unavailable energy in a closed thermodynamic system that is also usually considered to be a measure of the system's disorder, that is a property of the system's state, and that varies directly with any reversible change in heat in the system and inversely with the temperature of the system. All compounds undergo regular thermal decomposition in their final stages, and  $\Delta G$  energy Gibbs the standard Gibbs free energy change,  $\Delta G^\circ$ , indicates the thermodynamic favorability of a physical or chemical process. When  $\Delta G^\circ < 0$ , the

process is thermodynamically favored. For a given process, the value of  $\Delta G^\circ$  can be calculated directly from the values of  $\Delta H^\circ$  and  $\Delta S^\circ$  using the following equation:  $\Delta G^\circ = \Delta H^\circ - T\Delta S^\circ$ , processing is thermodynamically favored, as shown in Table.4 Figs. 12-15. Thermal study of ligand and some complexes are done using TGA (thermogravimetric analysis) and DSC curves. TGA measures the mass change of a substance with temperature when subjected to a controlled thermal program in a specific time. The obtained curve is referred to as a thermogravimetric curve and gives information about thermal stability, reaction rates, chemical structure, and the thermal stability of the products. The thermal behavior of ligand ( $H_4L$ ) and some of its complexes were characterized using thermogravimetric analysis curve (TGA). Schemes 7-10, Table.5 and Fig. 16,17 give identical results with suggested chemical formula of ligand ( $H_4L$ ) and tested complexes, and also demonstrate information for each pyrolysis step that occurred<sup>30, 31</sup>.

**Table 4. Differential scanning calorimetric data for ligand and some complexes**

Compound	$T_i/^\circ\text{C}$	$T_f/^\circ\text{C}$	Max. T. point $^\circ\text{C}$	$\Delta H$ J/g	$\Delta S$ J	$\Delta G$ J	Type
$C_{14}H_{12}N_2O_5$ ( $H_4L$ )	387.65	395.13	7.48	-3.43	-0.4588	-183.463	endothermic
$C_{14}H_{10}N_2O_5Co$	67.21	128.67	61.46	-89.78	-1.4607	-231.86	endothermic
$C_{14}H_{10}N_2O_7Mo$	49.17	65.49	16.32	-1.25	-0.0764	3.3	exothermic
	60.63	98.89	38.26	-25.63	-0.6698	25.904	exothermic
	172.41	257.74	85.33	54.25	0.6357	-89.12	endothermic
$C_{14}H_{12}N_2O_6ClRh$	46.17	63.49	56.51	-1.33	-0.0235	-0.002	endothermic
	60.34	98.63	76.54	-23.33	-0.3048	152.618	exothermic
	172.41	257.74	223.54	54.84	0.2453	0.01	exothermic
$C_{14}H_{12}N_2O_6ClCr$	324.45	334.99	332.57	-3.13	-0.0094	-0.004	endothermic
	41.08	106.52	65.44	-41.45	-0.6334	0.867	exothermic
	127.85	172.88	45.03	-18.41	-0.4088	43.19	exothermic
	182.36	196.21	13.57	-1.33	-0.0980	17.265	exothermic
	218.64	305.41	86.77	238.78	2.7516	-462.245	endothermic

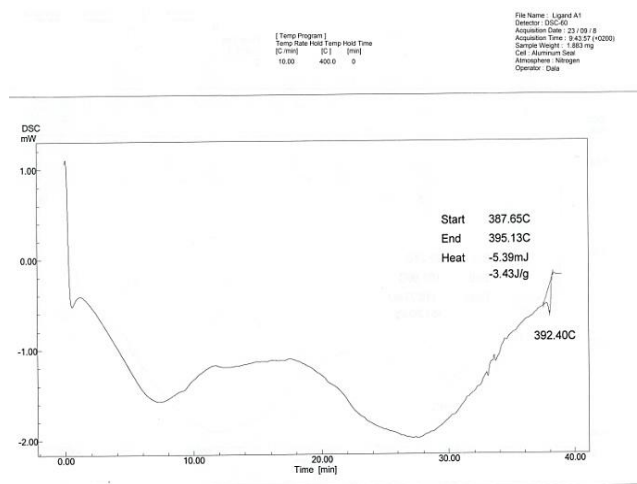


Figure 12. DSC. Curve for ligand (H<sub>4</sub>L)

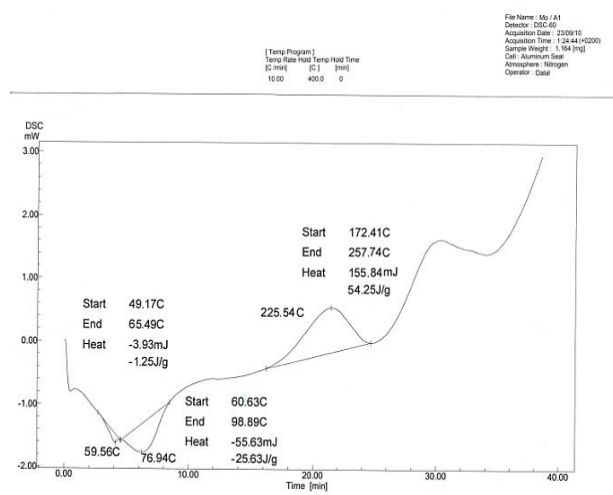


Figure 14. DSC. Curve for Mo-complex

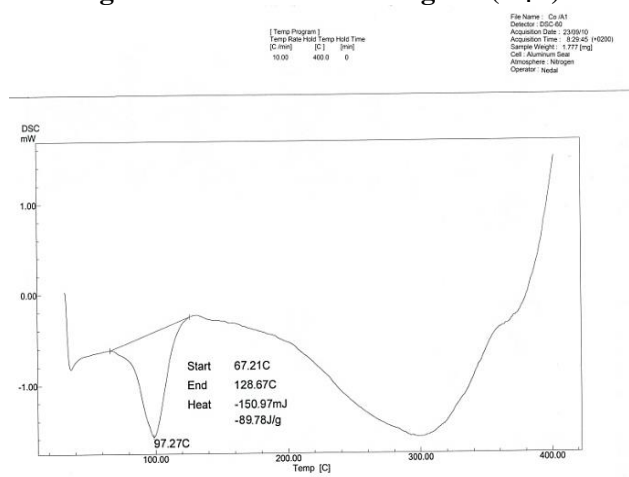


Figure 13. DSC. Curve for cobalt complex

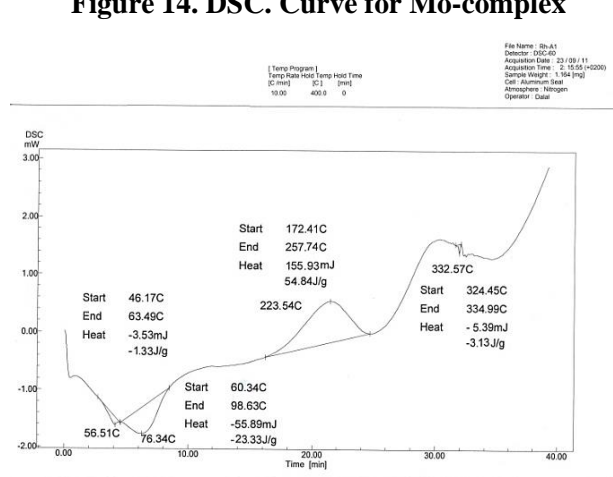
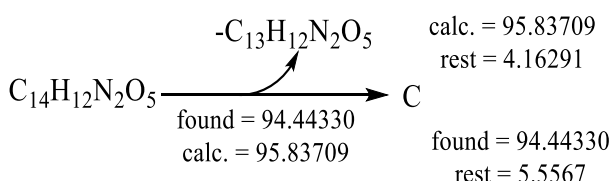


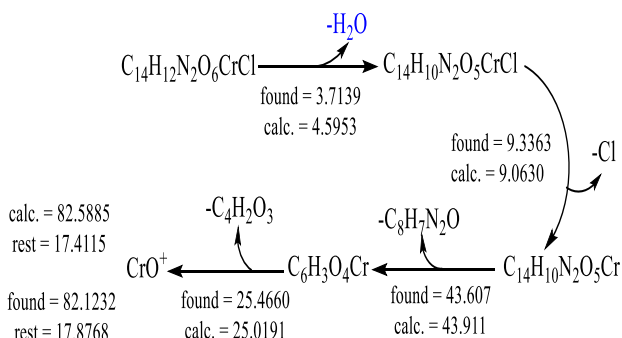
Figure 15. DSC. Curve for Rh-complex

Table 5. Thermo gravimetric analysis data for ligand and some complexes

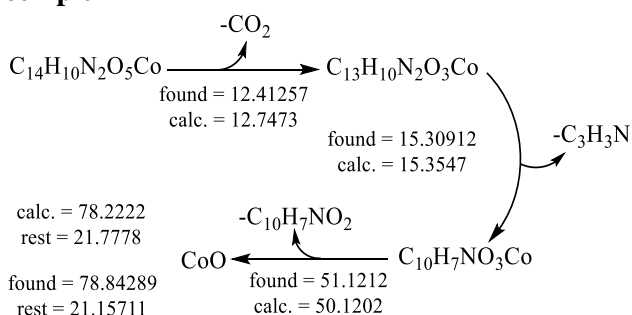
Compound (M. wt.)	% Estimated (calculated)		Assignment
	Mass loss	Total mass loss	
C <sub>14</sub> H <sub>12</sub> N <sub>2</sub> O <sub>5</sub> (H <sub>4</sub> L)	94.4433 (95.837)	94.4433 (95.837)	-C <sub>13</sub> H <sub>12</sub> N <sub>2</sub> O <sub>5</sub> C
	Calculated: 95.837% final = 4.16291%; Estimated 94.4433 % final = 5.5567%		
C <sub>14</sub> H <sub>12</sub> N <sub>2</sub> O <sub>6</sub> ClCr	(4.5953) 3.7139 (9.0630) 9.3363 (43.911) 43.607 (25.0191) 25.4660	82.1232 (82.588)	-H <sub>2</sub> O, -Cl -C <sub>8</sub> H <sub>7</sub> N <sub>2</sub> O -C <sub>4</sub> H <sub>2</sub> O <sub>3</sub>
	Calculated: 82.5885% final = 17.4115%; Estimated 82.1232% final = 17.8768%		
C <sub>14</sub> H <sub>10</sub> N <sub>2</sub> O <sub>5</sub> Co	(12.7473) 12.4125 (15.3547) 15.3091 (50.1202) 51.1212	78.84289 (78.222)	-CO <sub>2</sub> -C <sub>3</sub> H <sub>3</sub> N -C <sub>10</sub> H <sub>7</sub> NO <sub>2</sub>
	Calculated: 78.222% final = 21.7778%; Estimated 78.84289% final = 21.15711%		
C <sub>14</sub> H <sub>10</sub> N <sub>2</sub> O <sub>7</sub> Mo	(28.0071) 27.76457 (45.4312) 44.90801	73.10577 (72.520)	-2CO <sub>2</sub> , -N <sub>2</sub> -C <sub>12</sub> H <sub>10</sub> O <sub>2</sub>
	Calculated: 72.91511% final = 27.4796%; Estimated 73.10577 % final = 26.89423%		
C <sub>14</sub> H <sub>12</sub> N <sub>2</sub> O <sub>6</sub> ClRu	(12.1375) 12.8495 (27.2244) 26.6927 (34.0305) 33.47845	73.02065 (73.3924)	-H <sub>2</sub> O, -Cl -C <sub>6</sub> H <sub>4</sub> N <sub>2</sub> O -C <sub>8</sub> H <sub>6</sub> O <sub>3</sub>
	Calculated: 73.3924% final = 26.6076%; Estimated 73.02065% final = 26.97935%		



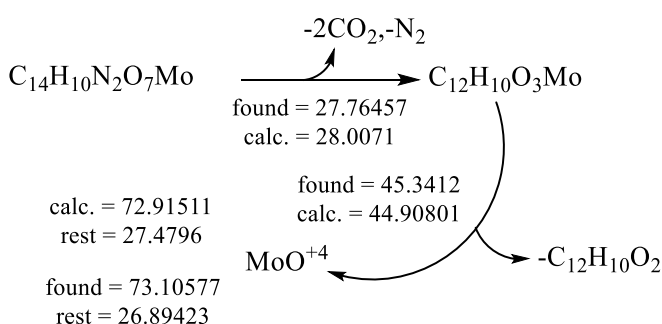
**Scheme 7. Pyrolysis pathway for ligand (H<sub>4</sub>L)**



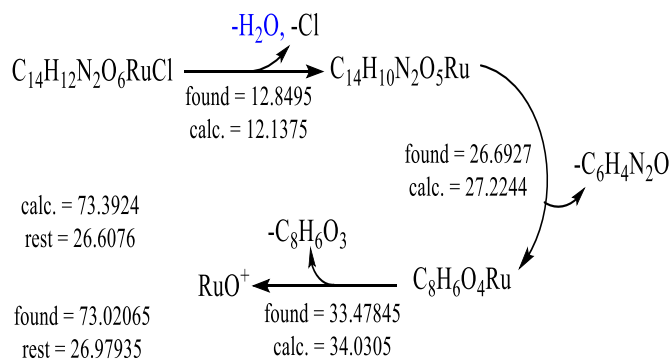
**Scheme 8. Pyrolysis pathway for chromium complex**



**Scheme 9. Pyrolysis pathway for cobalt complex**



**Scheme 10. Pyrolysis pathway for molybdenum complex**



**Scheme 11. Pyrolysis pathway for ruthenium complex**

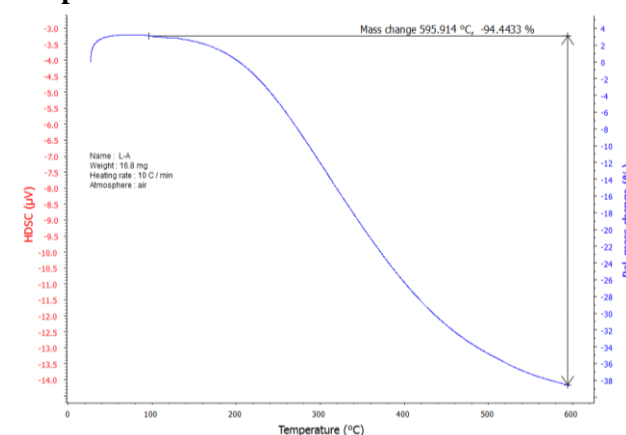


**Figure 16. thermogram of ligand (H<sub>4</sub>L)**

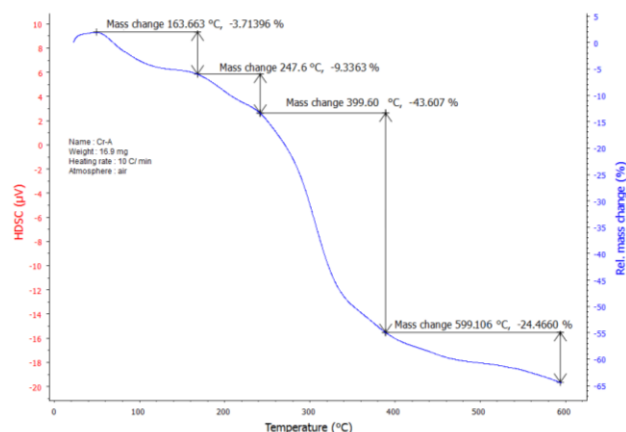


**Figure 17. thermogram of Cr- complex**

### Determination of DPPH Radical Scavenging Efficiency

The inhibitory effect of ligand H<sub>4</sub>L and its minerals, including Cr (III), Mo (VI), Fe (III), Ru (III), and Rh (III), on reactive oxygen species was evaluated using DPPH. The combination of the ligand and its minerals causes a change in color of DPPH from purple to yellow due to the transfer of hydrogen from the ligand to the DPPH molecule. The

color conversion was detected using a UV-Vis spectrophotometer at 517 nm. The inhibitory activity of the ligand H<sub>4</sub>L and its minerals on reactive oxygen species was ranked in the following order: (H<sub>4</sub>L>Ascorbic acid > Mo-H<sub>2</sub>L> Fe-H<sub>2</sub>L> Cr-H<sub>2</sub>L > Rh-H<sub>2</sub>L> Ru-H<sub>2</sub>L) based on the higher IC<sub>50</sub> value indicating lower antioxidant effectiveness, as shown in Fig. 18 after 30 minutes. The ligand and molybdenum complex demonstrated higher antioxidant activity. The free radical scavenging effects of all the compounds with the DPPH radical

were evaluated using the following equation and presented in Table.6 under the same conditions<sup>32, 33</sup>.

$$PI \% = \frac{\text{Absorbance of control} - \text{Absorbance of sample}}{\text{Absorbance of control}} \times 100\%$$

PI = Percentage Inhibition

RSA = 100 – PI; : RSA = Radical Scavenging Activity

**Table 6. Radical scavenging activities, Percentage Inhibition and IC<sub>50</sub> values**

Compound	Conc. µg/ml	PI %	RSA %	IC <sub>50</sub>	Compound	Conc. µg/ml	PI %	RSA %	IC <sub>50</sub>			
C <sub>14</sub> H <sub>12</sub> N <sub>2</sub> O <sub>5</sub> (H <sub>4</sub> L)	0.375	9.95	90.05	0.019	Mo-Complex	0.374	15.94	84.06	0.026			
	0.186	42.17	57.83			0.186	48.89	51.11				
	0.093	58.99	41.01			0.093	67.11	32.89				
	0.046	66.08	33.92			0.046	74.95	25.05				
	0.374	33.94	66.06			0.374	30.70	69.30				
Cr-Complex	0.186	55.88	44.12	0.127	Rh- Complex	0.186	45.86	54.14	0.132			
	0.093	69.03	30.97			0.093	54.49	45.51				
	0.046	73.94	26.06			0.046	59.98	40.02				
	0.374	26.62	73.38			0.113	69.48	30.52				
	0.186	42.28	57.72			0.057	84.38	15.62				
Fe- Complex	0.093	48.95	51.05	0.125	Ru- Complex	0.028	89.49	10.51	0.189			
	0.046	51.99	48.01			0.013	94.38	5.62				
	<b>Compound</b>					<b>Conc. µg/ml</b>	<b>PI %</b>	<b>RSA %</b>		<b>IC<sub>50</sub></b>		
	<b>Ascorbic acid</b>					0.374	12.29	87.80		0.023		
						0.186	36.75	63.25				
					0.03	58.74	41.26					

**Variations of IC<sub>50</sub> for the ligand and its complexes**

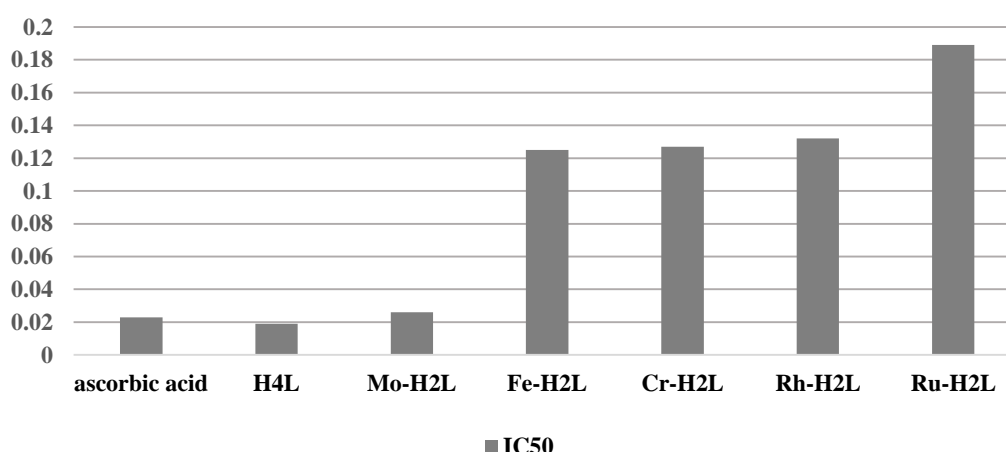


**Figure 18. Variations of IC<sub>50</sub> values for H<sub>4</sub>L ligand and its complexes**

## Conclusion

A novel azo ligand was prepared *via* the reaction of the diazonium salt of 3-aminophenol with 2, 4, 6-trihydroxy acetophenone. This ligand was then employed to access new complexes with

different metals. These complexes were identified using a number of analytical techniques, such as elemental microanalysis, metal chloride-containing, electrical conductivity measurement, magnetic

susceptibility,  $^1\text{H}$ - and  $^{13}\text{C}$ -NMR, FT-IR, and UV-Vis spectroscopy. Calculations of the thermodynamic parameters  $\Delta\text{H}$ ,  $\Delta\text{S}$ , and  $\Delta\text{G}$  were made using the DCS curve, and the atomic N, O, and O tetradentate coordination sites in the ligand were identified by comparing their FT-IR spectra to those of the metal complexes. The M:L ratio in every compound was 1:1. The dye used the complexes prepared from it to determine their ability to inhibit

free radicals by measuring their ability as antioxidants using DPPH as a free radical and D-ascorbic acid as a standard substance and determining the value of  $\text{IC}_{50}$ . The ligand exhibited a significant capacity to suppress free radicals, and its ability to inhibit the complexes varied depending on the  $\text{IC}_{50}$  value. The results are as follows:  $\text{H}_4\text{L} > \text{Ascorbic acid} > \text{Mo-complex} > \text{Fe-complex} > \text{Cr-complex} > \text{Rh-complex} > \text{Ru-complex}$ .

## Acknowledgment

Authors would like to thank everyone that contributed to the success of this review article Department of Chemistry, College of Science for

Women, University of Baghdad, Ministry of Higher Education & Scientific Research & Science and Technology, Directorate of Environment & Water.

## Author's Declaration

- Conflicts of Interest: None.
- We hereby confirm that all the Figures and Tables in the manuscript are ours. Furthermore, any Figures and images, that are not ours, have been included with the necessary permission for re-publication, which is attached to the manuscript.

- Ethical Clearance: The project was approved by the local ethical committee at Ministry of Education.
- Ethics statement:
- No animal studies are present in the manuscript.
- No human studies are present in the manuscript.
- No potentially identified images or data are present in the manuscript.

## Authors' Contributions Statement

This work carried out in collaboration between all authors. A. M. F. prepared the samples, wrote and edited the manuscript with revision. A. A. S. did the

tests and interpreted the data with revision and S. G. M. did the tests of antioxidants and listed their data in the manuscript.

## References

1. Mohammed H. Synthesis, identification, and biological study for some complexes of azo dye having theophylline. *Sci World J.* 2021 Jul 22; vol. 2021:9. <https://doi.org/10.1155/2021/9943763>
2. Mahmudov KT, Gurbanov AV, Aliyeva VA, Resnati G, Pombeiro AJ. Pnictogen bonding in coordination chemistry. *Coord Chem Rev.* 2020 Sep 1; 418: 213381. <https://doi.org/10.1016/j.ccr.2020.213381>
3. Hamza IS, Mahmmoud WA, Al-Hamdani AA, AhmedSD, Allaf AW, Al Zoubi W. Synthesis, characterization, and bioactivity of several metal complexes of (4-Amino-N-(5-methyl-isaxazol-3-yl)-benzenesulfonamide). *Inorg Chem Commun.* 2022; 144: 109776.
4. El-Gammal OA, Mohamed FS, Rezk GN, El-Bindary AA. Synthesis, characterization, catalytic, DNA binding and antibacterial activities of Co (II), Ni (II) and Cu (II) complexes with new Schiff base ligand. *J Mol Liq.* 2021; 15(326): 115223. <https://doi.org/10.1016/j.molliq.2020.115223>
5. El-Gammal OA, El-Bindary AA, Mohamed FS, Rezk GN, El-Bindary MA. Synthesis, characterization, design, molecular docking, anti COVID-19 activity, DFT calculations of novel Schiff base with some transition metal complexes. *J Mol Liq.* 2022; 15(346): 117850. <https://doi.org/10.1016/j.molliq.2021.117850>
6. Khedr AM, El-Ghamry H, Kassem MA, Saad FA, El-Guesmi N. Novel series of nanosized mono-and homobi-nuclear metal complexes of sulfathiazole azo dye ligand: Synthesis, characterization, DNA-binding affinity, and anticancer activity. *Inorg. Chem. Commun.* 2019; 1(108): 107496. <https://doi.org/10.1016/j.inoche.2019.107496>
7. Al-Hassani RA. Synthesis, Characterization, Antimicrobial and Theoretical Studies of V (IV), Fe (III), Co (II), Ni (II), Cu (II), and Zn (II) Complexes with Bidentate (NN) Donor Azo Dye Ligand.

- Baghdad Science Journal. 2016 Dec 4;13(4):0793-  
<https://doi.org/10.21123/bsj.2016.13.4.0793>.
8. Kirthan BR, Prabhakara MC, Naik HB, Nayak PA, Naik EI. Synthesis, characterization, DNA interaction and anti-bacterial studies of Cu (ii), Co (ii) and Ni (ii) metal complexes containing azo-dye ligand. Chem Data Collect. 2020 Oct 1; 29: 100506. <https://doi.org/10.1016/j.cdc.2020.100506>
  9. Turan N, Buldurun K, Adiguzel R, Aras A, Turkan F, Bursal E. Investigation of spectroscopic, thermal, and biological properties of FeII, CoII, ZnII, and RuII complexes derived from azo dye ligand. J Mol Struct. 2021 Nov 15; 1244: 130989. <https://doi.org/10.1016/j.molstruc.2021.130989>
  10. Abdallah SM, Zayed MA, Mohamed GG. Synthesis and spectroscopic characterization of new tetradentate Schiff base and its coordination compounds of NOON donor atoms and their antibacterial and antifungal activity. Arab J Chem. 2010; 3(2): 103-13. <https://doi.org/10.1016/j.arabjc.2010.02.006>
  11. Kumar DN, Garg BS. Synthesis and spectroscopic studies of complexes of zinc (II) with N<sub>2</sub>O<sub>2</sub> donor groups. SAA. Spectrochim Acta - A: Mol Biomol. 2006; 64(1) Ma: 141-7. <https://doi.org/10.1016/j.saa.2005.07.008>
  12. Sahar YJ, Mohammed HS. Synthesis and characterization some complexes of azo dye of pyrimidynyl and evaluating their biological activity. QJPS. 2019; 24(3). <https://doi.org/10.29350/qjps.2019.24.3.970>
  13. Deghadi RG, Mahmoud WH, Mohamed GG. Metal complexes of tetradentate azo-dye ligand derived from 4, 4-oxydianiline: Preparation, structural investigation, biological evaluation and MOE studies. Appl Organomet Chem. 2020; 34(10): e5883. <https://doi.org/10.1002/aoc.5883>
  14. Al Zoubi W, Ko YG. Self-assembly of hierarchical N-heterocycles-inorganic materials into three-dimensional structure for superior corrosion protection. J Chem Eng. 2019; 356: 850-6. <https://doi.org/10.1016/j.cej.2018.09.089>
  15. Kareem MJ, Al-Hamdani AAS, Jirjees VY, Khan ME, Allaf AW, Al Zoubi W. Preparation, spectroscopic study of Schiff base derived from dopamine and metal Ni (II), Pd (II), and Pt (IV) complexes, and activity determination as antioxidants. J Phys Org Chem. 2021; 34(3): e4156. <https://doi.org/10.1002/poc.4156>
  16. Hadi MA, Kareem IK. synthesis, Characterization and Spectral Studies of a new Azo-Schiff base Ligand Derived from 3, 4-diamino benzophenone and its Complexes with Selected Metal Ions. J Adv Sci. 2020; 1(1). <https://royalliteglobal.com/rjas/article/view/251>
  17. Waheeb AS, Kyhoiesh HA, Salman AW, Al-Adilee KJ, Kadhim MM. Metal complexes of a new azo ligand 2-[2'-(5-nitrothiazolyl) azo]-4-methoxyphenol (NTAMP): Synthesis, spectral characterization, and theoretical calculation. Inorg. Chem. Commun. 2022; 138: 109267. <https://doi.org/10.1016/j.inoche.2022.109267>
  18. Deswal Y, Asija S, Dubey A, Deswal L, Kumar D, Jindal DK, et al. Cobalt (II), nickel (II), copper (II) and zinc (II) complexes of thiazazole based Schiff base ligands: Synthesis, structural characterization, DFT, antidiabetic and molecular docking studies. J Mol Struct. 2022 Apr 5; 1253: 132266. <https://doi.org/10.1016/j.molstruc.2021.132266>
  19. Al-Khateeb ZT, Karam FF, Al-Adilee K. Synthesis and characterization of some metals complexes with new heterocyclic azo dye ligand 2-[2'-(5-Nitrothiazolyl) azo]-4-methyl-5-nitro phenol and their biological activities. J Phys Conf Ser. 2019; 1294(5): 052043. IOP Publishing. <https://doi.org/10.1088/1742-6596/1294/5/052043>
  20. Jaber SA, Kyhoiesh HA, Jawad SH. Synthesis, characterization and biological activity studies of cadmium (II) complex derived from azo ligand 2-[2'-(5-bromo Thiazolyl) azo]-5-dimethyl amino benzoic acid. J Phys Conf Ser. 2021; 1818(1): 012013. <https://doi.org/10.1088/1742-6596/1818/1/012013>
  21. Dahi MA, Jarad AJ. Synthesis, characterization and biological evaluation of thiazolyl azo ligand complexes with some metal ions. J Phys Conf Ser. 2020; 1664(1): 012090. <https://doi.org/10.1088/1742-6596/1664/1/012090>
  22. Mohamed MG, EL-Mahdy AF, Kotp MG, Kuo SW. Advances in porous organic polymers: Syntheses, structures, and diverse applications. Mater Adv. 2022; 3(2): 707-33. <https://doi.org/10.1039/D1MA00771H>
  23. Alhakimi AN, Shakdofa MM, Saeed S, Shakdofa AM, Al-Fakeh MS, Abdu AM, et al. Transition Metal Complexes Derived from 2-hydroxy-4-(p-tolyldiazenyl) benzylidene)-2-(p-tolylamino) acetohydrazide Synthesis, Structural Characterization, and Biological Activities. J Korean Chem. Soc. 2021; 65(2): 93-105. <https://doi.org/10.5012/jkcs.2021.65.2.93>
  24. Al-Hamdani AAS, Al-Alwany TAM, Mseer MA, Fadhel AM, Al-Khafaji YF. Synthesis, Characterization, Spectroscopic, Thermal and Biological Studies for New Complexes with N1, N2-bis (3-hydroxyphenyl) Oxalamide. Egypt J Chem. 2023; 66(4): 223-235. <https://doi.org/10.21608/EJCHEM.2022.144403.6297>
  25. Kyhoiesh HA, Al-Adilee KJ. Synthesis, spectral characterization, antimicrobial evaluation studies and cytotoxic activity of some transition metal complexes with tridentate (N, N, O) donor azo dye ligand. Results Chem. 2021; 3: 100245. <https://doi.org/10.1016/j.rechem.2021.100245>

26. Al-Daffay RK, Al-Hamdani AA, Al Zoubi W. Synthesis, Characterization and Thermal Analysis of Cu (II), Co (II), Ru (III) and Rh (III) Complexes of a New Acidic Ligand. *Ibn al-Haitham J Pure Appl Sci.* 2023 Oct 20; 36(4): 321-37. <https://doi.org/10.30526/36.4.3047>
27. Jain S, Dongare K, Nallamotheu B, Dora CP, Kushwah V, Katiyar SS then et al. Enhanced stability and oral bioavailability of erlotinib by solid self nano emulsifying drug delivery systems. *Int J Pharm.* 2022; 622: 121852. <https://doi.org/10.1016/j.ijpharm.2022.121852>
28. Asim N, Amin MH, Alghoul MA, Sulaiman SN, Razali H, Akhtaruzzaman M, et al. Developing of chemically treated waste biomass adsorbent for dye removal. *J Nat Fibers.* 2021 Jul 3; 18(7): 968-77. <https://doi.org/10.1080/15440478.2019.1675214>
29. Shaalan N. Preparation, Spectroscopy, Biological Activities and Thermodynamic Studies of New Complexes of Some Metal Ions with 2-[5-(2-Hydroxy-Phenyl)-1, 3, 4-Thiadiazol-2-Ylimino]-Methyl-Naphthalen-1-Ol]. *Baghdad Sci J.* 2022; 19(4): 0829-0837. <http://dx.doi.org/10.21123/bsj.2022.19.4.0829>
30. Abdulridah M Q, Al-Hamdani A A S, Hussen IA. Synthesis, Characterization and Antioxidant Activity of New Azo Ligand and Some Metal Complexes of Tryptamine Derivatives. *Baghdad Sci. J.* 2023; 20(3 suppl.): 1046-1063. <https://doi.org/10.21123/bsj.2023.8227>
31. Hasan M. Synthesis, Identification, and Biological Study for Some Complexes of Azo Dye Having Theophylline. *Sci World J.* 2021; 76(3): 1-9. <https://doi.org/10.1155/2021/9943763>
32. Al-Daffay R. Kh., Al-Hamdani A. A. S," Synthesis, Characterization, and Thermal Analysis of a New Acidicazo Ligand's Metal Complexes. *Baghdad Sci. J.* 2023;20(1): 121-133. <https://doi.org/10.21123/bsj.2022.6709>
33. Al Zoubi W, Al-Hamdani AAS, Duraid Ahmed S, Basheer HM, Al-Luhaibi RS, Dib A. Synthesis, characterization, and antioxidant activities of imine compounds. *J Phys Org Chem.* 2019 Mar; 32(3): e3916. <https://doi.org/10.1002/poc.3916>

## تحضير وتشخيص ودراسة مضادات الاكسدة لمعقدات ايونات بعض العناصر مع ازو 1-(2،4،6)- ثلاثي هيدروكسي-3-(3-هيدروكسي فنيل) ثنائي زينيل) فنيل) ايثان-1-اون

اريج ملك فاضل<sup>1</sup>، عباس علي صالح الحمداني<sup>2</sup>، سعد كوما محمد<sup>3</sup>

<sup>1</sup>وزارة التربية، مديرية تربية بغداد، بغداد، العراق.

<sup>2</sup>قسم الكيمياء، كلية العلوم للبنات، جامعة بغداد، بغداد، العراق.

<sup>3</sup>قسم هندسة التعدين والمعادن معهد التبين للدراسات المعدنية، القاهرة، مصر.

### الخلاصة

اثناء تفاعل الديزنة تكونت صبغة أزو جديدة عن طريق تفاعل 3-امينوفينول مع 2،4،6-ثلاثي هيدروكسي اسيتوفينون . ثم تم تفاعل هذا الليكاند مع بعض ايونات العناصر الكروم والحديد الروديوم والروثينيوم بتكافؤهم الثلاثي والكوبلت الثنائي والموليبدنيوم سداسي التكافؤ مكونة معقدات فلزية مختلفة بأشكال هندسية متعددة. تم ملاحظة تناسق مجموعة الازو مع ايونات العناصر من خلال ملاحظة ظهور حزم امتصاص الفلز مع النتروجين والاكسجين بتقنية مطيافية الاشعة تحت الحمراء مشيرة إلى ارتباط النتروجين والأكسجين مباشرة مع الفلز. تم تعيين الازان الجزيئية لليكاند ومعقداته باستخدام مطيافية الكتلة وكذلك تم عمل تحليل للعناصر. تم قياس حزم امتصاص الاطياف الالكترونية لتحديد الشكل الهندسي للمعقدات , اضافة الى ذلك تم تحديد استقرارية المركبات من حيث احتواءها على جزيئات الماء من عدمه باستخدام تقنيتي المسح الحراري التفاضلي التحليل الحراري الوزني تم قياس تأثير المعقدات كمضادات اكسدة اتجاه 2،2-داي فينيل بكريل هيدرازيل (DPPH) وهو عبارة عن جذر حر مستقر الذي يتم استخدامه لمعرفة فعالية كسح الجذور الحرة لنوع الاوكسجين النشطة ولوحظ التالي (H<sub>4</sub>L > Ascorbic acid > Mo-Complex > Fe-Complex > Cr-Complex > Rh-Complex > Ru-Complex) خلال ثلاثون دقيقة . اختبار DPPH قام باختزال الالكترن المنفرد لذرة النتروجين عن طريق استلام ذرة هيدروجين من المعقدات المضادة للأكسدة لتكوين الهيدرازين المقابل . نتيجة الفحص تراوحت ما بين قيم تثبيط لمركبات نشطة وغير نشطة تم ادراجها في البحث.

**الكلمات المفتاحية:** 3-امينو فينول, 2،4،6-هيدروكسي اسيتوفينون، الفعالية، مضادات الاكسدة، التحلل الحراري الوزني، صبغة الازو.